Advances in Water Resources 81 (2015) 186–198

Contents lists available at ScienceDirect

Advances in Water Resources

journal homepage: www.elsevier.com/locate/advwatres

A sediment fluxes investigation for the 2-D modelling of large river morphodynamics

Massimo Guerrero [a,*], Francisco Latosinski [b], Michael Nones [c], Ricardo N. Szupiany [b], Mariano Re [d], Maria Gabriella Gaeta [c]

[a] Hydraulic Engineering Laboratory, Department of Civil Chemical Environmental and Materials Engineering, University of Bologna, via Terracini, 40131 Bologna, Italy
[b] Faculty of Engineering and Water Sciences, International Centre for Large River Research (CIEGRI), Littoral National University, Santa Fe City, Santa Fe, CP 3000, CC 217, Argentina
[c] Research Centre for Constructions-Fluid Dynamics Unit, University of Bologna, via Terracini, 40131 Bologna, Italy
[d] Hydraulics Laboratory, National Institute for Water (INA), Ezeiza, Argentina

ARTICLE INFO

Article history:
Available online 10 February 2015

Keywords:
Parana River
ADCP
Dune-tracking
2-D modelling
River morphodynamics
Sediment transport calibration

ABSTRACT

A complete understanding of alluvial-bed dynamics is desirable for evaluating a variety of issues related to water resources.

Sediment fluxes were investigated in a bifurcation of the large Parana River near Rosario, Argentina. The backscatter estimations from the Doppler profilers provided the suspended load of the sediment forming the riverbed. An echo-sounder was applied to track the dunes yielding the bed-load estimation.

Aiming to show the usefulness of the recorded data, a 2-D numerical code was applied to the 10-km long and 2-km wide Rosario reach. The morphodynamic module was un-coupled from the hydrodynamics assessment, which enabled the long-term prediction of the river morphology accounting for the hydrological yearly variation with a quasi-steady approach.

Numerical experiments were performed to test the sensitivity of the hydrodynamic model to the computational time-step and mesh size, to test the un-coupling scheme performance regarding the full-dynamic modelling, to test the accuracy of the sediment transport formulae based on the field evidence and, finally, to provide guidance to properly fix the model parameters.

1. Introduction

The transport of the sediment forming the riverbed has been widely studied to understand the alluvial bed dynamics and its reciprocal feedback with the hydrodynamics. The sediment transport is commonly classified based on the following dominant mechanisms: the bed-load is referred to as the transport occurring near the riverbed in which the stream flow sweeps the bed particles over the underlying sand bedforms or the gravel bed and the suspended load in which the particles are transported fully suspended in the water column. The suspended-load, containing the finer particles, often represents the majority of the transported sediments reaching the sea; therefore, the measurement technologies have primarily focused on the flux of the suspended materials [1–7]. However, the morphology of large rivers is also influenced by sand fluxes close to the bottom.

Detailed and frequent measurements of the sediment transport in a river stream-flow are desirable for the evaluation of many issues related to river hydro-morphodynamics, such as the effects of climate change on the river morphology and the riverine habitat, the safety of the civil engineering structures (e.g., bridges and embankments), and the maintenance of the navigation channels and hydropower intakes. River sediment transport and deposition–erosion patterns are primarily responsible for determining the channel morphology of large rivers [8,9]. The sediment that feeds the delta at the river outlet serves to build coastal landforms and maintain the shoreline [10–13].

The Parana River represents an important waterway for the South America region of the La Plata Basin, which joins parts of Argentina, Bolivia, Brazil, Paraguay and Uruguay. Therefore, the dynamics of the water and sediment along this watercourse has been studied by various authors, with the principal aim of clarifying the interrelationships among the climate, hydrology, riverine hydraulics and morphology, which affect the water resources and fluvial structures, such as bridges, ports and levees [14,15].

Over the last years, field techniques and analytical or numerical models have been applied to study these interactions along

* Corresponding author. Tel.: +39 0512090519; fax: +39 0512090518.
E-mail addresses: massimo.guerrero@unibo.it (M. Guerrero), franlatos@gmail.com (F. Latosinski), nones@gerstgraser.de (M. Nones), rszupiany@yahoo.com.ar (R.N. Szupiany), mre@fi.uba.ar (M. Re), g.gaeta@unibo.it (M.G. Gaeta).

http://dx.doi.org/10.1016/j.advwatres.2015.01.017
0309-1708/

Notation

a	reference level for the sediment concentration assessment over the riverbed
C	Chézy parameter ($m^{1/2}/s$)
C'	specific skin friction parameter
C_b	river bars celerity
cr	morphodynamic model compression rate
d	sediment diameter (m)
D	normalised particle diameter
f	correction factor for suspended-load concentration
g	gravitational acceleration (m/s^2)
$\overline{h}$	average dune height (m)
h	water depth (m)
H	water level (m)
$hd\text{-}ts$	hydrodynamic time-step (s)
hev	horizontal eddy viscosity (m^2/s)
k	total-load calibration coefficient
k_b	bed-load calibration coefficient
k_l	suspended-load calibration coefficient
L	dune wave length
L_b	river bars wave length
$md\text{-}ts$	morphodynamic time-step (s)
$md\text{-}st$	morphodynamics to the sediment transport time scales ratio
$p-q$	mass flux variables in the grid s–n directions
P	sand porosity
Q_{ref}	flow discharge (m^3/s)
R_n	radius of curvature, direction n
R_s	radius of curvature, direction s
RHS	Reynolds stresses
s–n	computational grid directions
s	relative density of the sediment to the water
sf	morphodynamic model scale factor
S	total sediment transport rate
S_b	bed-load
S_l	suspended-load
S_s	sediment transport flux, direction s
S_n	sediment transport flux, direction n
T	oscillation period of local flow velocity
u	local flow velocity (m/s)
u'_*	effective friction velocity over the grains
v_m	migration velocity (m/day)
z	bed level
ϑ'	shields parameters
Δu	oscillation amplitude of local flow velocity
ϑ_c	critical shields parameter
τ	shear stress
τ''	bedforms drag
τ'	skin friction

the sandy rivers [2,16,17]. New methodologies [18–20] have overcome the traditional limited measurement devices used in the past; consequently, the data taken by these new methods may assist the numerical models simulation for a better understanding of the riverbed dynamics. Innovative instrumentations employed in river surveys include Acoustic Doppler Current Profilers (ADCPs), which could be used to characterise the secondary flows and the vertically averaged velocity patterns [22,22], to evaluate the shear stress by fitting the logarithmic velocity profiles [16,23] and to study the suspended-load [2,7,24]. Concerning the sand-beds, acoustic technologies have also been applied to track the bedforms, eventually estimating the bed-load. This approach for dune tracking consists of applying a single or multi-beam echo-sounder in repeated surveys to measure the dune geometries and their translation lengths [26–30].

In the present study, acoustic techniques were applied to estimate the sediment fluxes in the Parana River near Rosario, Argentina, discerning among the sediment grain sizes and the dominant transport mechanisms (i.e., suspended and bed-load). The used devices (i.e., the ADCPs and a single-beam echo-sounder) were easily deployed compared with traditional samplers and provided detailed data for the monitoring and forecasting of the sediment fluxes and the resulting morphology. Aiming to show the usefulness and applicability of these data, the river channel morphodynamics was simulated with an existing two dimensional (2-D) numerical model (Mike21C by the Danish Hydraulic Institute-DHI [32]), assuming the shallow water approximation.

In more detail, the single- and multi-frequency backscatter techniques were applied to characterise the suspended-load of the sand forming the riverbed, whereas the bed-load was estimated by tracking the dunes with a single-beam echo-sounder in the same field campaign.

The 2-D hydro-morphodynamic model simulated the water–sediment flow and the bed level interaction by applying an un-coupled and quasi-steady approach. In the computations, the yearly discharge variations in the river were considered, and the morphology of the channels was accurately represented.

A wide sensitivity analysis was performed regarding the effect of the time steps, the computational grid and the adopted transport formulae on the resulting morphology. The acoustic surveys provided the reference data, in previously unrated detail, for the calibration of the sediment transport formulae implemented in the numerical model (i.e., the total-load formula has been given by Engelund and Hansen [33] and the suspended- and bed-load formulae by van Rijn [34,34]).

This accurate modelling will foster an efficient management of the river to meet the objectives, such as the navigation channel maintenance.

The paper is organised as follows. The next section presents the materials and methods, with a particular focus on the study site, the applied measurement techniques and the mathematical model. This section also briefly introduces the performed numerical simulations, focusing on the available historical data, i.e., the stage-discharge relationship, the water level records and the river morphology maps, which were used as the boundary conditions and for the model set up. Section 3 reports the achieved results in terms of the estimated sediment fluxes in the field, the numerical model parameters from the sensitivity analyses and the morphology calibration. Aiming to provide a general guidance for the numerical modelling of large river morphodynamics, the outcomes of these analyses are then discussed in Section 4, highlighting the following: (i) the dependence of the model parameters on the observed morphological features, (ii) the usefulness and limits of the estimation of the sediment fluxes using acoustic backscatter. The concluding remarks are reported in the final sections.

This study extended our investigation regarding the Parana River: the interconnections among the applied methods, and the previous and current results and objectives are outlined in Fig. 1.

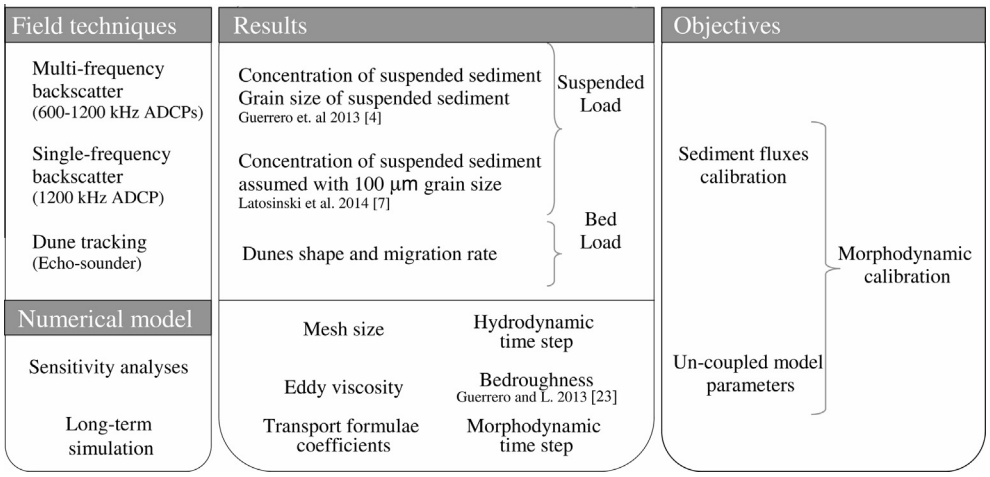

Fig. 1. Structure of the presented study.

2. Materials and methods

2.1. Study site

The Parana River has a watershed that covers approximately 2.6×10^6 km^2 and is one of the largest rivers in the world [36], with a total length of approximately 4900 km, and outflows into the Atlantic Ocean near the city of Buenos Aires (Fig. 2(a)). The Middle and Lower reaches flow from north to south through Argentina for approximately 1000 km (Fig. 2(b)) and have a mean annual discharge of approximately 12,000–15,000 m^3/s, a water surface slope on the order of 10^{-5} and a total sediment transport of approximately 130–135 $\times$ 10^6 t/year [8,36]. A significant portion of this transport (approximately 80%) is considered as wash-load coming from the Bermejo River, a tributary of the Paraguay River flowing from the Andes. The remaining portion, composed of sand (Fig. 2(c)), shapes the bed of the river and is classified as suspended load and bed load. The planform pattern of the Parana River channels is classified as anabranching with braided/meandering thalweg [36–37].

The present investigation of the sediment fluxes was conducted in the large expansion-bifurcation unit, which is located in the lower reach of the watercourse near Rosario, 420 km from the delta (Fig. 2(d)). This unit was in the upstream portion of the numerical domain that spanned a 10-km long reach, including the bifurcation, the sand bar obstructing the meandering channel, and the large island between the two channels.

2.2. Field measurements

The site was surveyed on November 16 and 17, 2010 when the total flow discharge Q_{ref} was equal to 14,320 m^3/s. The bed and the suspended sediment samples were obtained at four fixed measuring verticals (s1, s2, s3 and s4 in Fig. 2(d)) positioned across the 2.3-km-wide, 14-m-mean-depth river cross section upstream of the bifurcation where the following acoustic measurements were also performed: (i) the ADCPs profiling to evaluate the suspended-load of the sand across the section, and (ii) the single-beam echo-sounder longitudinal profiling to estimate the displacement of the bedforms from the dune tracking.

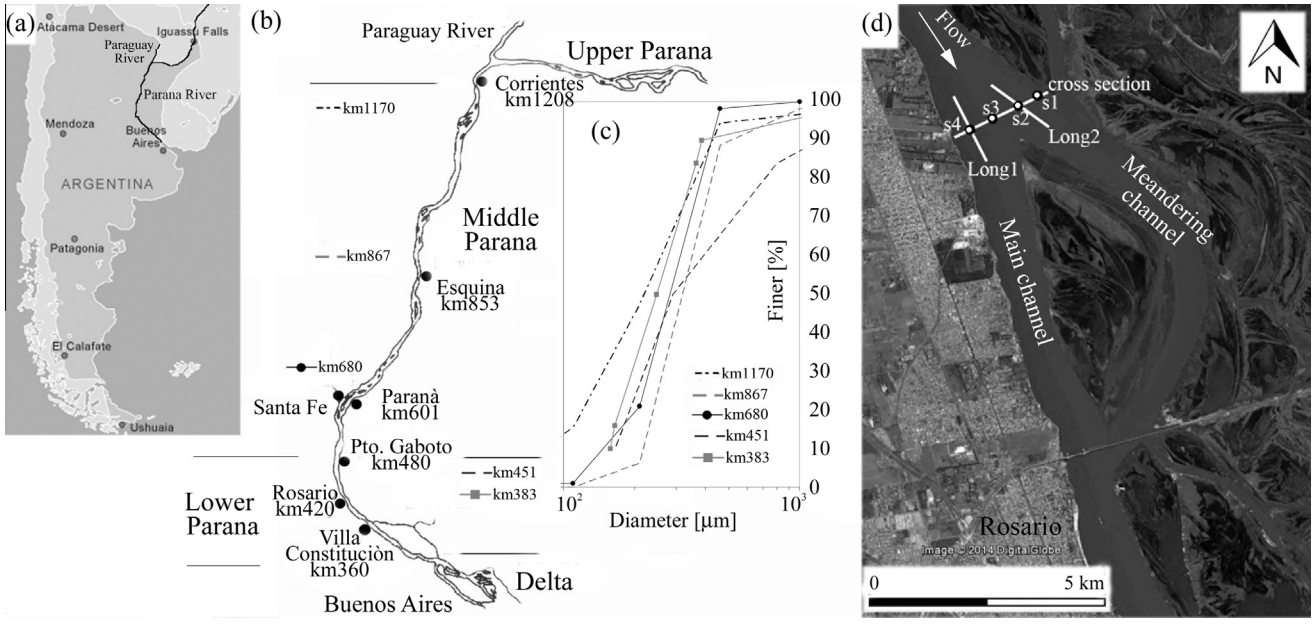

Fig. 2. The Argentina's map with the Parana River (a); the Middle and Lower Parana River (b); sediment distributions of samples from the riverbed (c), located with respect to the distance of the navigation way from Buenos Aires in Fig. 2b; the studied reach (d) of the Lower Parana River near Rosario.

The application of the acoustic backscatter by deploying the ADCPs in the riverine environment to infer the profile concentrations have been applied by various authors [2–7]. Among others, Guerrero et al. [2] have first compared the single to the multi-frequency ADCPs method in the large Parana River, showing that the latter also provides grain size profiles. In the other studies regarding the Parana River, Guerrero et al. [4] have provided the calibration of the multi-frequency method using the sand contents of the samples, and Latosinski et al. [7] have calibrated the single-frequency method.

However, regardless of the applied approach, the recorded echo from the ADCP is corrected for a variety of reasons (e.g., beam spreading and sound attenuation); therefore, it is correlated to the backscatter from the suspended sand with different limits related to the accounted grain size and the concentration that, finally, depends on the used frequencies. The evaluations of the sediment concentration and the grain size (the latter is possible only using the multi-frequency) using the measured backscatter is referred to as the inverse problem, whereas the direct problem consists of modelling the backscatter by applying the known sediment features that yield the calibration of the ADCPs. The inverse and the direct problems were successfully solved at the bifurcation cross section (Fig. 2(d)) by applying the 1200-kHz-frequency [7] and the 600–1200 kHz pair of frequencies [4]. In the present study, the findings of these previous applications were further analysed to compare the sediment fluxes of the different sand fractions, finally achieving the numerical model calibration.

The dune tracking was performed by applying an echo-sounder in repeated surveys to measure the dune geometries and their translation lengths along the thalweg of the two channels over approximately 24 h. The longitudinal sections (Long. 1 and Long. 2 in Fig. 2(d)) in the main channel and the meandering channel were 650 and 500 m long, respectively. These profiles crossed seven dunes along the right channel and fifteen dunes along the other channel, therefore showing different dune wave lengths.

The dune tracking method [39] was applied to each of the observed dunes to estimate the sediment transport rate in m^2/day, as follows:

$$g_{sf} = 0.66 \cdot (1 - P) \cdot \overline{h} \cdot v_m \tag{1}$$

where 0.66 is a shape factor, P is the sand porosity, v_m is the estimated migration velocity in m/day, and $\overline{h}$ is the average dune height, observed over two consecutive profiles of the same dune.

2.3. The mathematical modelling

Open source and proprietary codes are available to simulate the morphodynamics of watercourses with fixed and movable beds. Generally, large rivers have a width-to-depth ratio ranging from 10 to 100. Therefore, the shallow water approximation could be applied in these cases leading to a depth-integrated or 2-D model. The commercial 2-D code, Mike21C, developed by the DHI [32] presents certain advantages to simulate the morphodynamics of large rivers. The space and time resolutions may be adapted to a variety of cases, eventually un-coupling the hydrodynamic from the morphological-time-step, leading to reasonable computational times, even in cases of large computational domains, such as in the Parana River case study.

Mike21C includes the two-dimensional Navier–Stokes equations for the liquid phase, which are the conservation of momentum in two directions (Eqs. (2) and (3), respectively) and the continuity of mass (Eq. (4)). These equations are solved on a curvilinear grid with the s–n directions and the $R_s - R_n$ radii of curvatures using an implicit finite difference scheme [32,39,40].

$$\frac{\partial p}{\partial t} + \frac{\partial}{\partial s}\left(\frac{p^2}{h}\right) + \frac{\partial}{\partial n}\left(\frac{pq}{h}\right) - 2\frac{pq}{hR_n} + \frac{p^2 - q^2}{hR_s} + gh\frac{\partial H}{\partial s} + \frac{g}{C^2}\frac{p\sqrt{p^2+q^2}}{h^2} = RHS \tag{2}$$

$$\frac{\partial q}{\partial t} + \frac{\partial}{\partial s}\left(\frac{pq}{h}\right) + \frac{\partial}{\partial n}\left(\frac{q^2}{h}\right) + 2\frac{pq}{hR_s} - \frac{q^2 - p^2}{hR_n} + gh\frac{\partial H}{\partial s} + \frac{g}{C^2}\frac{q\sqrt{p^2+q^2}}{h^2} = RHS \tag{3}$$

$$\frac{\partial H}{\partial t} + \frac{\partial p}{\partial s} + \frac{\partial q}{\partial n} - \frac{q}{R_s} + \frac{p}{R_n} = 0 \tag{4}$$

The mass flux variables ($p - q$) in the s–n directions, the water depth h and the level H are defined over a space staggered computational grid. The hydrodynamic model neglects the lateral exchange of the momentum due to water friction and the gradients of the vertical velocity, i.e., the pressure distribution is considered to be hydrostatic. Given these limitations, the numerical code is suited to represent small gradients in water surface entailing small Froude numbers and small ratios of water depth to curvature radius. The Reynolds stresses are described in the right hand side (*RHS*) terms of Eqs. (2) and (3), including the horizontal turbulence viscosity (i.e., horizontal eddy viscosity). This macro-turbulence parameter was calibrated over the range of 2–10 m^2/s to maintain a stable computation over the entire domain of the case study. The Chézy parameter, C, is typically calibrated to simulate the bed roughness effect on the velocity field.

Aiming to investigate the reciprocal feedbacks between the river channel morphology and the sediment fluxes, a detailed numerical modelling of the Rosario reach was conducted using Mike21C. An un-coupled approach was applied that enabled a reliable simulation of the long-term changes in the observed river morphology.

The morphodynamics model combines the hydrodynamic with the sediment transport calculations; the flow field is continuously updated according to the morphology changes of the bed. The un-coupled approach entails the solution of the hydrodynamics prior to the continuity equation for the sediment (Eq. (5)).

$$(1 - P)\frac{\partial z}{\partial t} + \frac{\partial S_s}{\partial s} + \frac{\partial S_n}{\partial n} - \frac{S_n}{R_s} + \frac{S_s}{R_n} = 0 \tag{5}$$

A space centred, time forwarded, explicit, difference scheme is applied to solve Eq. (5), where z and $S_s - S_n$ are the bed level and the sediment transport fluxes in the s–n directions, respectively. The solution of this latter equation gives the new bed morphology, and then the hydrodynamic model proceeds with the next time step.

A relevant advantage of the un-coupled approach is the use of different time steps for the liquid and sediment phases. The long-term simulation of the morphodynamics of large rivers would be extremely demanding in terms of computational resources when using fully dynamic models. In this case, the governing equations for the two phases are coupled into one set of differential equations, which are concurrently solved by applying an individual time step. This time step is limited to fulfil the most demanding Courant criteria, which is for the liquid phase. The water and bed level waves are characterised by celerities with different orders of magnitude; generally, the hydrodynamics is computed using the time steps of a few seconds, whereas the morphological changes occur over long periods (from days to years).

The un-coupled approach uses different time steps and solution strategies tailored over appropriate temporal scales of the simulated processes. In this case study, the hydrodynamics was solved adopting an implicit finite difference scheme with a Courant number of approximately four, whereas the transient solution of the

riverbed was computed with an explicit scheme, which was characterised by a small Courant number. Therefore, a scale factor (*sf*) defined as the ratio between the morphodynamic and hydrodynamic-time-step (*md-ts* and *hd-ts*, respectively) was introduced.

Two different approaches are available in the applied code to un-couple the morphodynamic and hydrodynamic modules (*md-m* and *hd-m*, respectively) that fix the value for *sf*. One method consists of alternatively marching the two modules with different time steps but maintaining the same frequency, i.e., the *one-to-one* time step approach. This approach compresses the hydrodynamic events with a rate (*cr*) equal to *md-ts* over *hd-ts*, which, in this case, corresponds to *sf*. The other available method is to activate *md-m* with a lower frequency with respect to *hd-m*, that is, one over *md-ts* (i.e., the *low-frequency* approach), which, in this case, is the inverse ratio of *sf*. These two methods may be combined or individually applied; however, quasi-steadiness in hydrodynamics is required. Consequently, the boundary conditions should slowly vary over time because the morphological-hydrodynamic reciprocal adaptations could occur before the following hydrological condition forces a new morphology configuration. Therefore, a sensitivity analysis (described in Section 3.2) was conducted on the effect of the adopted *sf* in the morphology results.

Regarding the performed long-term simulations, the calibration of the adopted sediment transport formulae noticeably influenced the resulting morphology. Therefore, numerical experiments (described in Section 3.3) were conducted to investigate the reliability of the sediment transport formulae combined with different representations of the bed composition. In more detail, the model proposed by Engelund and Hansen [33] is a total-load formula, which was adopted to represent the bed composition with an individual grain size of 250 μm, which is the D_{50} of the sediment forming the riverbed in the simulated reach. Alternatively, the van Rijn formulae for the suspended- and bed-load assessments [33,34] respectively were assumed in combination with a graded model that included the two most frequent classes observed in the riverbed (i.e., 125 and 250 μm).

The Engelund and Hansen model was implemented in the code as reported in Eq. (6), where S is the total sediment transport rate, C and ϑ' are the Chézy and Shields parameters [42], respectively, s is the relative density of the sediment to the water, g is the gravitational acceleration, d is the sediment diameter, and k is a calibration coefficient.

$$S = k \cdot 0.05 \frac{C^2}{g} \vartheta'^{\frac{5}{2}} \sqrt{(s-1) \cdot g d^3} \tag{6}$$

The Shields parameter ϑ (Eq. (7)) is defined as the ratio between the shear stress, τ, over the riverbed and the relative weight of the sediment grains forming the riverbed in which the former (Eq. (8)) is estimated with the local flow velocity, u, and the Chézy parameter C.

$$\vartheta = \frac{\tau}{\rho g \cdot (s-1) \cdot d} \tag{7}$$

$$\tau = \rho g \frac{u^2}{C^2} \tag{8}$$

The shear stress is typically divided into bedforms drag τ'' and skin friction τ'. The shear stress due to skin friction produces sediment transport, whereas τ'' gives rise to bedforms, i.e., dunes in the large Parana River. In the code, the estimation of the skin friction using Eq. (9) combines with the Engelund–Hansen formula (Eq. (6)) to provide the total-load assessment.

$$\vartheta' = 0.06 + 0.4 \cdot \vartheta^2 \tag{9}$$

The dependence of ϑ' on the Chézy parameter, through Eq. (7), eventually yielded a sediment transport overestimation. Indeed, the Chézy parameter was fixed based on the expected alluvial roughness and the consequent bedform drag to achieve a proper hydrodynamic calibration rather than an accurate sediment transport assessment. However, the calibration coefficient k in Eq. (6) was applied to correct the transport rate estimation.

The van Rijn model for the bed-, S_b, and suspended-load, S_l, assessments was implemented in the code with Eqs. (10) and (11), respectively, where u'_* is the effective friction velocity over the grains estimated in Eqs. (12) and (13), and ϑ_c is the critical Shields parameter, depending on the normalised particle diameter D (Eq. (14)).

$$S_b = k_b \cdot 0.053 \cdot \left(\frac{u'^2_*}{\vartheta_c \cdot (s-1) \cdot g d^3} - 1 \right)^{2.1} \cdot \frac{\sqrt{(s-1) \cdot g d^3}}{D^{0.3}} \tag{10}$$

$$S_l = k_l \cdot f \cdot \left[0.015 \cdot \left(\frac{u'^2_*}{\vartheta_c \cdot (s-1) \cdot g d^3} - 1 \right)^{1.5} \cdot \frac{d}{a \cdot D^{0.3}} \right] \cdot u \cdot h \tag{11}$$

$$u'_* = \frac{u \sqrt{g}}{C'} \tag{12}$$

$$C' = 18 \log_{10} \left(\frac{4h}{d} \right) \tag{13}$$

$$D = d \cdot \left(\frac{s-1}{v} g \right)^{\frac{1}{3}} \tag{14}$$

The level, a, in Eq. (11) is assumed to be equal to the maximum between 1% of water depth, h, and two times the assumed grain size of the sediment forming the riverbed, d. This level is the reference level for the sediment concentration assessment over the riverbed (i.e., the square brackets term). In the same equation, f is a correction factor accounting for the actual distribution of the suspended sediment concentration over the depth. This correction factor is evaluated based on the Rouse suspension parameter [43]. An advantage of the van Rijn model implementation is that the effective friction velocity does not depend on the Chézy parameter, C, but on a specific skin friction parameter, C', which represents the actual roughness due to the grain size (Eq. (13)). However, the coefficients $k_b - k_l$ may be defined to calibrate Eqs. (10) and (11).

The van Rijn model enabled the representation of the individual contributions of the sediment fractions to different sediment mechanisms. In this case, the graded model option was activated, and the riverbed composition was described. With this option, the transport formulae were individually evaluated for each of the represented sediment classes and were reduced based on the corresponding percentages in the riverbed composition.

2.4. The case study implementation

The computational grid was tailored over the observed morphological features and changes. The curvilinear grid was made by adapting its borders to the actual planimetric configuration of the main channel and the meandering channel on the left side next to the large alluvial plain (Fig. 3). Finally, the computational mesh was fixed to the average size of 100 × 50 m^2 with a higher resolution (40 × 20 m^2) where the maximum stream flows were expected, i.e., in the channels rather than over the islands (with approximately 200 m grid spacing), for a total of approximately 11,000 nodes. Grid smoothing was applied to provide uniform grid weights, especially among the channels (15% variation), while, simultaneously, the deviation from the orthogonal grid was maintained within fifteen degrees.

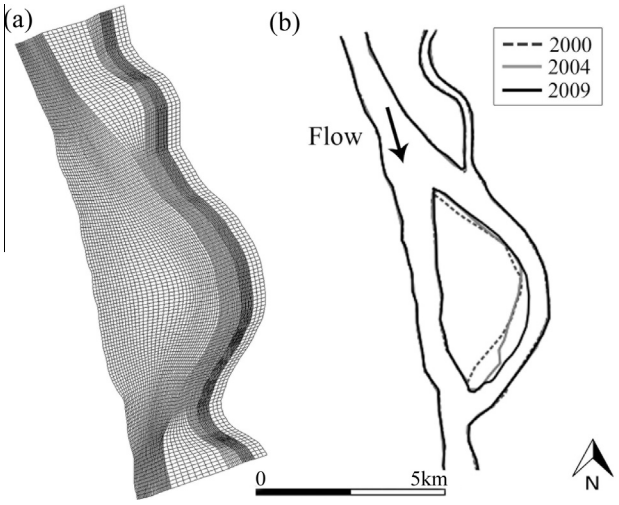

Fig. 3. The computational grid for the 2-D numerical simulations (a) and the island shorelines during the period 2000–2009 (b), derived by the analysis of satellite images [44].

Aiming to account for the dunes roughness, which is the primary contributor to producing the shear stress close to the riverbed, Eq. (15) was adopted for the Chézy parameter, as follows:

$$C \cdot \sqrt{g} = 36 \cdot h^{\frac{1}{6}} \tag{15}$$

where h is the local water depth. This formulation was calibrated by Guerrero and Lamberti [24] to accurately simulate the flow field with the wetted region limited to the active channels, such as for the majority of the time from 2004 to 2009.

The bathymetries and river shoreline surveys of 2004–2009 provided evidence of a progressive avulsion of the meandering reach (Fig. 3(b)) that resulted in an overall deepening of the right channel by approximately 1 m and the widening of the central island towards the alluvial plain by approximately 100 m.

This field evidence yielded a rough estimation of the celerity of the developing bars to be within the orders of 10^{-1} to 10^{-3} m/day during the wet months. Given these low rates of changes, the *md-m* was successfully uncoupled from *hd-m*, finally adopting 3 h and 20 s as the *md-ts* and *hd-ts*, respectively. In agreement with this approach, the quasi-steady boundary conditions were applied to simulate the yearly hydrology variation. This approach represents the slow changes in the river channel morphology, which is particularly suited to the physics of the case study but does not directly simulate the dune formation and propagation, because they are characterised by a higher celerity. These small scale processes were indirectly accounted for using the roughness parameter (Eq. (15)) and the sediment transport formulae.

Therefore, eighty-seven steady hydrological conditions were sequentially imposed at the model boundaries; they spanned the entire simulated period (2004–2009) and lasted approximately 20–25 days each, representing the actual variation of the flow discharge with sufficient detail (Fig. 4). Moreover, a period of 20 days is two orders of magnitude longer than the *md-ts*, which was sufficient to accurately simulate a morphological steady solution within each sub-period. Additional days were simulated merging the steady sub-periods, eventually representing the yearly variations in the simulated series (Fig. 4(a)). The rate of these variations was 10^3 m^3/day.

Concerning this quasi-steady approach, the performed sensitivity analysis provided reasonable deviations from the morphology resulting from a fully dynamic simulation (i.e., *md-ts* equal to *hd-ts*) as described in Section 3.2.

The flow discharges and water levels, imposed as the model boundary conditions, were derived from the daily records of the water levels in Chapeton, where an accurate discharge-level relationship is maintained, and in Rosario at the computation domain downstream-end. Chapeton is located close to the Santa Fe-Parana crossing, 160 km upstream from Rosario (Fig. 2(b)). This distance introduced a lag of a few days between the actual and the imposed discharge in the upstream boundary that was neglected when applying the quasi-steady approach. During the analysed period, the daily discharges in Chapeton and the water levels in Rosario varied over the ranges of 11,000–27,000 m^3/s and 4.4–8.7 m, respectively.

A constant sediment transport rate equal to zero was imposed at the upstream boundary to roughly represent the erosion process observed over the last decades in the main channel [45].

The single grain size and the graded model options were alternatively applied. In the first case, the Engelund and Hansen model was used, and the bed material was represented by a 250 μm grain size. In the other case, the two most frequent classes observed in the riverbed (i.e., 125 and 250 μm) were used with the same percentage (i.e., 50%) to describe the bed composition. The graded model was coupled with the van Rijn formulae for the bed and the suspended-load; the coarse fraction was attributed to the bed-load mechanism, whereas the suspended-load accounted for both of the classes. Very fine sand, silt and clay were not represented in this study because these sediment fractions were not observed with significant amounts in the bed samples (Fig. 2(c)).

3. Results

3.1. Evidence from the field measurements

The sand fractions from a recent collection of samples of the riverbed resulted in a nearly homogeneously distributed along the Middle and Lower Parana reaches, ranging over 100–1000 μm, with a median diameter of approximately 300 μm; the variation of the average distribution was characterised by D_{84} and D_{16} grain sizes of 400–190 μm, respectively (Fig. 2(c)). The bed samples collected on November 16 and 17, 2010 within the modelled area resulted in a median grain size D_{50} equal to 250 μm, with the average distribution characterised by D_{84}–D_{16} values equal to 400–130 μm and spanning the range of 100–400 μm. Significantly more medium-fine sand was present in the sampled water columns during the same campaign with the total flow discharge Q_{ref}. The analysis on these samples resulted in values of D_{84}, D_{50} and D_{16} equal to 134, 100 and 75 μm, respectively.

The backscatter measured by a 1200 kHz ADCP provided the estimation of the sediment concentration over the range of 40–300 μm that assumed the backscatter from the particles within this range to be equivalent to the backscatter from the corresponding D_{50} value (i.e., 100 μm). A more accurate modelling of the sand backscatter [4] was used in the double-frequency method by applying the echoes at the 600–1200 kHz frequencies from the same water column. In this case, the inverse problem was solved, yielding the concentrations of the fractions coarser than 80–90 μm. These different assumptions were reflected in the evaluated sand fluxes. The resulting transport rate of the suspended sand in the cross section (Fig. 2(d)) was approximately 268 kg/s using the 1200 kHz single-frequency and decreased to approximately 74 kg/s when combining the actual grain sizes with the corresponding concentrations (using the 600–1200 kHz frequency pair).

The evaluated values of the suspended-load were 1.2–1.5 times larger when considering the extrapolations of the investigated concentration and the velocity fields to the unmeasured areas from the ADCPs, i.e., near the bottom and the water surface, which yielded

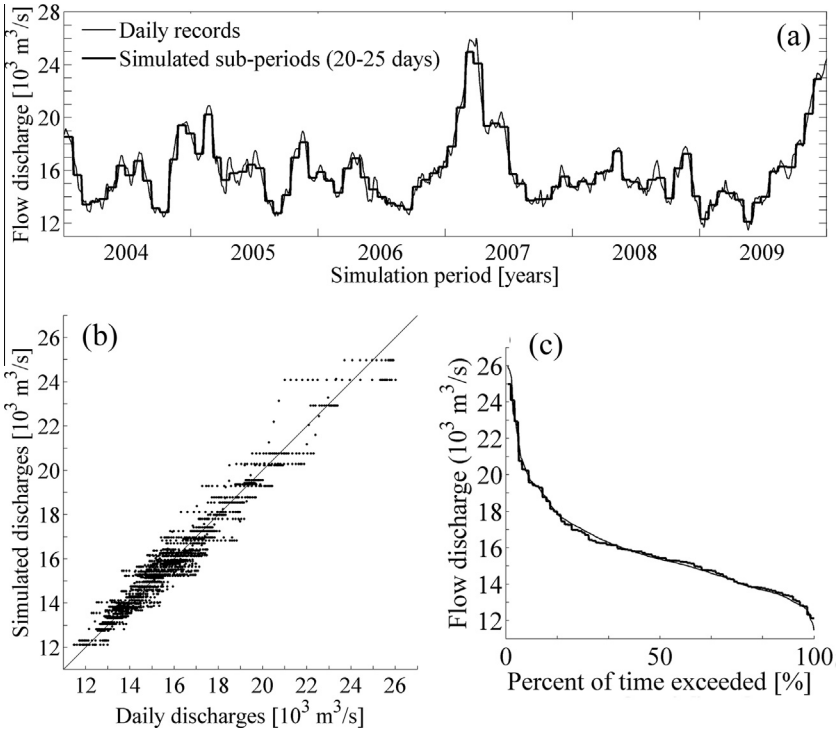

Fig. 4. Flow discharge time series at the upstream boundary of the numerical model: daily and quasi-steady values (a); comparison between the two series in terms of flow discharge values (b) and corresponding distributions (c).

406 and 89 kg/s (corresponding to the average concentration of 28 and 6 mg/l) for the single and double-frequency estimations, respectively.

The two frequencies method also provided evidence on the distribution of the investigated concentration field among the different grain size classes in the surveyed cross section. The coarse fractions were particularly evident among the shallow part of the cross section close to the sand bar obstructing the meandering channel (positions S1 and S2 in Fig. 2(d)). Fine sand (125 μm) and low concentrations were observed in the stream flow core (positions S3 and S4 in Fig. 2(d)) within 12–8 m of the water depth. Regarding the sediment mass distribution in the observed grain sizes, the sand over the range of 80–200 μm represented 75% of the total mass, and the remainder was over the range of 200–300 μm; the D_{84}, D_{50} and D_{16} values were equal to 213,148 and 101 μm, respectively.

The dune tracking along the two channels (Long. 1 and 2 in Fig. 2(d)) gave an average rate of the forms displacement of 2.8 m/day and a variability of 0.7 m/day as the standard deviation (Fig. 5). The observed rates of the dunes displacement did not show a clear correlation with the observed dune heights (Fig. 5(c)), whereas the dune height and the length appeared relatively well correlated with the water depth. These morphological parameters were 1.5 m and 130 m for the 15-m-deep main stream, and 0.7 and 43 m in the 5-m-deep secondary channel. Longitudinal transects were performed along the thalweg of the two channels that may have the highest dunes across the river section, whereas the averaged values along the section were roughly estimated from the undulation observed in the profile along the same cross section surveyed with the ADCPs. This analysis gave an averaged dune height and width that changed from 1.1 to 0.3 m and from 126 to 78 m, respectively, passing from the main stream to the secondary channel. The bed-load was finally evaluated by applying in Eq. (1) the average rate of the dune displacement from the two performed longitudinal transects and the estimated dune heights along the cross section profile. The resulting values further multiplied the corresponding widths, which gave the cumulative estimations of the bed-load as 21.7 kg/s and 1.6 kg/s for the main and secondary channels, respectively.

3.2. Sensitivity analysis of the numerical model parameters

Numerical tests are typically performed to validate the modelling tools [46], which entail sensitivity analyses of the model parameters most affecting the final result (e.g., the computational mesh size and the irregularity, time step length, and interpolation functions of the variables). Although Mike21C by DHI is a well-tested code and its validation is not the goal of this study, the numerical investigation of the long-term variation of the large river morphology requires a series of simplifications that were carefully tested regarding the Parana study.

An initial series of numerical experiments concerned the *hd-m* module; the stability of the resulting velocity and water level fields was investigated against the choice of computation mesh size, horizontal turbulence viscosity (i.e., horizontal eddy viscosity, *hev*) and *hd-ts* length. Two averaged longitudinal sizes of the computational mesh were tested, 100 and 50 m along with three time steps of 20, 15 and 10 s, and three values for *hev* (2, 5 and 10 m^2/s). The entire period of 2004–2009 was simulated.

Less than 1% of change in the resulting velocity fields was observed by varying the time step. The local instabilities in the velocity field were produced in the case of a smaller *hev* and large flow discharges that eventually crashed the computations. Therefore, a *hev* value of 10 m^2/s was finally fixed to avoid the local spikes corresponding to the computational grid irregularities. The refinement of the computational mesh, on average, gave less than 1% of change in the resulting velocity field and even a smaller change was observed in the water levels.

Regarding the optimum combination of *hev* and the mesh size, the horizontal scale of the river-flow macro-eddies was considered.

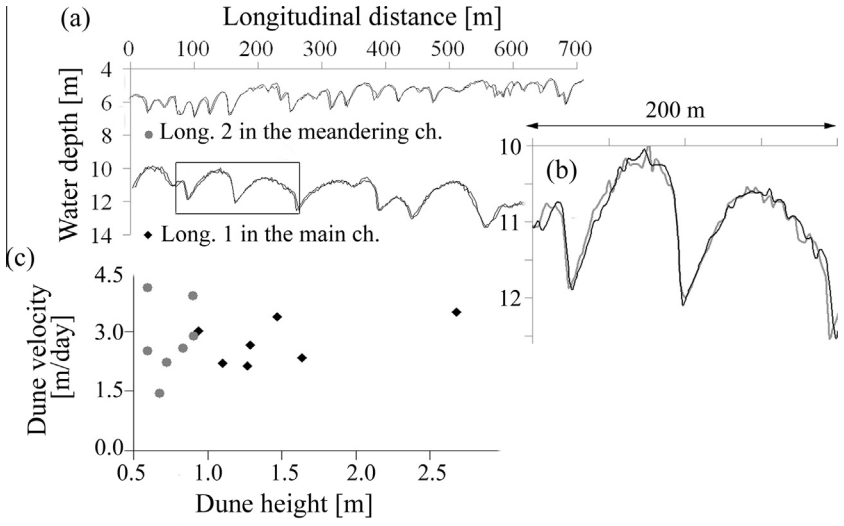

Fig. 5. Dune profiles (a) from the field survey performed in the main channel (Long. 1) and in the meandering channel (Long. 2); a detail from the profiling in two consecutive days (b). The dune migration velocities over the corresponding heights (c).

This turbulence oscillation is primarily related to the dune wave length [47]. The dune wave lengths of approximately 50 and 100 m were observed in the main and the meandering channels, respectively (Fig. 5). Moreover, oscillations with a period and wave length of approximately 100 s and 100 m, respectively, were reported for the velocity-concentration field in the Rosario reach of the Parana River [4]. These periodicities were observed with velocity oscillations on the order of 10^{-1} m/s, which was approximately 10% of the velocity magnitude. Given these values, *hev* was estimated at approximately 50–100 times (i.e., the wave length of the observed periodicities) the order of magnitude of the observed velocity oscillations, and resulted equal to 5–10 m^2/s.

The ratio between the average mesh size of 100 m and the scale of horizontal plane eddies was close to unity in which the latter was estimated with the average velocity magnitude (i.e., 1.2 m/s) times the time scale of the observed periodicity (i.e., 100 s). This macro-turbulence scale also corresponded to the average dune length in the main channel.

Although the short scale diffusion was not directly represented, the eddy viscosity in the vertical alignment, i.e., along the water depth, was accounted for in the calibrations of the *hd-m* using the Chézy parameter.

A second computational testing focused on the *md-m* module, un-coupled from the *hd-m* to simulate two days with steady hydrological conditions corresponding to a discharge of 17,000 m^3/s. This discharge was one of the most frequent values larger than the average over the period from 2004 to 2009, which accumulated most of sediment load.

Both of the un-coupling approaches were tested (i.e., *one-to-one* and *low-frequency*) by comparing the resulting morphology from a fully dynamic simulation to the corresponding results from seven different combinations of *cr*, the *md-m* marching frequency and *sf*, as reported in Table 1. The required computational times for the simulations may be compared in the same table in terms of clock ticks (i.e., cycles) for a single processor CPU. The *hd-ts* was fixed to 20 s, whereas the un-coupling parameters yielded *md-ts* values ranging from one minute to six hours. The average longitudinal size of the computational mesh was 100 m.

The final deviations (i.e., biases) from the fully dynamic result were evaluated in terms of the differences in the bed levels averaged among the computational domain. These deviations ranged from 2% to 19%, primarily depending on *cr*, as summarised in Table 1.

The *sf* and consequent *md-ts* were fixed by the *md-m* frequency and the applied compression rate, *cr*, to hydrodynamics events. This rate characterises the *one-to-one* approach for the *md-m* un-coupling and appeared extremely effective in biasing the final morphology and simultaneously reducing the computational effort. However, when *sf* was increased by using a low frequency but maintaining a small compression rate of the hydrodynamic events, reasonable deviations were observed. Considering a more detailed analysis of the simulation results (Fig. 6), a large deviation was progressively introduced in the evaluated morphology for *cr* and *sf* equal to 15 (simulation md-01), which biased 19% of the final morphological change. In contrast, the bias due to the *md-m* un-coupling appeared to slowly reach 2% for the simulation of md-02, which was characterised by the same *sf* and *md-ts* as for md-01 (15 and 5 min, respectively); however, in this case, no compression was applied to the hydrodynamic events. The md-02 reduced the computational time to approximately half of the time used for the fully dynamic simulation, whereas the md-01 required only one tenth.

These differences clarified the advantage and the required computational resources when using the *low-frequency* rather than the *one-to-one* approach for the *md-m* un-coupling in the Parana case study. Nearly the same development as for the average bias of md-02 was observed for md-03 and md-04, but in the latter case, a significantly larger *md-ts* (1 h rather than 1 min) was used, which does not entail a significant computational time savings. The *low-frequency* approach does not reduce the *hd-m* computations proportionally to the *sf*, but the hydrodynamics is simulated with a marching time step equal to *hd-ts*, eventually reaching a steady configuration over the frozen morphology.

Progressing to an even larger *md-ts* (1–3 h for simulations md-05 to md-07), short period oscillations were observed due to the low frequency computation of the actual morphology. However, in the case in which *cr* is equal to 1 (md-05 and md-06), these oscillations appeared to decrease in amplitude while converging to a final deviation of a few percent at the end of the simulation.

An additional *md-m* run was performed with the same boundary conditions and the un-coupling parameters as for md-02 but using the finer computational mesh with an average longitudinal size of 50 m. Compared with the results obtained by the coarser computational grid, no relevant modifications (i.e., within 2%) were observed in the final morphology. The finer grid simulation

Table 1
Un-coupling parameters of the morphodynamic model *md-m*, the corresponding deviations from the fully dynamic model and the required computational time.

Simulation	*cr*	*md-m* frequency	*sf*	*md-ts*	Final dev. (%)	Single processor 10^9 clock ticks
Fully dynamic	1	1	1	20″	n.a.	177.5
md-01	15	1	15	5′	19	17.7
md-02	1	1/15	15	5′	2	69.8
md-03	3	1	3	1′	3	66.6
md-04	1	1/180	180	60′	3	60.5
md-05	1	1/540	540	180′	3	62.9
md-06	3	1/180	540	180′	8	20.6
md-07	1	1/1080	1080	360′	5	57.8

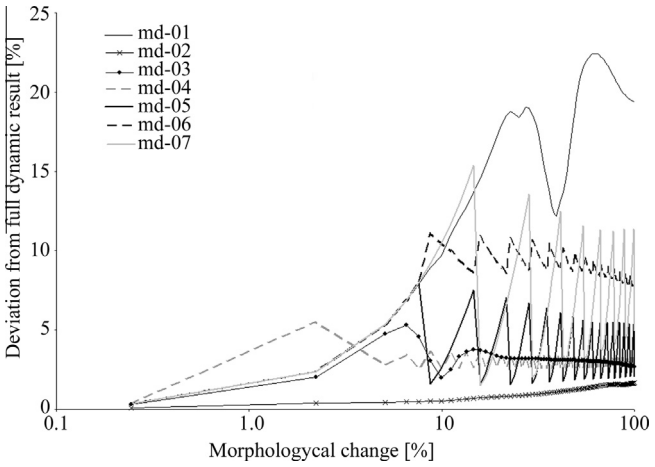

Fig. 6. The deviations from the fully dynamic results for different un-coupling parameters as reported in Table 1, versus the morphological change dynamically simulated and normalised over its final value.

resulted in a higher resolution of the bed representation that was not significant for the river bars and channels in the Rosario case study.

The goal of a third sensitivity analysis was to verify the morphological deviations due to the *md-m* un-coupling in the long-term. To this end, 30 days were dynamically simulated to be compared to the *low-frequency* un-coupled simulations of the same period with 1, 3 and 6 h *md-ts*. A relevant hydrological change was imposed at the boundaries to simulate the most demanding condition for the computation over the period from 2004–2009. The discharge was increased by 1000 m^3/s per day starting from 17,000 m^3/s up to 24,000 m^3/s and was then maintained at this high level for the remaining 23 days, which simulated the beginning of 2007 (Fig. 4(a)). The bias introduced in the evaluated morphologies by the un-coupling approach appeared nearly completely dissipated in approximately 10 days of the simulated period, i.e., in 3 days of the steady high discharge. The final deviation and the required computational time were proportional to the applied *md-ts* and its inverse ratio, respectively. Although no relevant differences were observed in the simulations characterised by an *md-ts* of 1 and 3 h, the final deviation of the evaluated morphology was within 1% for the latter case, which was a good compromise between the accuracy and the required computational resources.

3.3. Sensitivity analysis of the sediment transport formulae

The most relevant uncertainty in morphodynamics modelling concerns the accuracy of the applied sediment transport formulae. Especially in long-term simulations, even a small inaccuracy in the representation of the sediment fluxes may accumulate significant biases in the final morphology, whereas the accurate prediction of the bed level change is required for river management to meet the objectives, such as fluvial navigation and environmental sustainable hydro-powering.

Two widely accepted sediment transport models suited to sandy rivers were tested based on the field evidence regarding the sediment-loads (the ADCPs and dune-tracking surveys) and the morphology changes that occurred in the simulated period from 2004 to 2009. The Engelund and Hansen total-load formula was applied with a single fraction of 250 μm, which is the median diameter of the sediment forming the riverbed in the Rosario reach. This formula gave a reasonable prediction of the actual total-load (including the fractions larger than 40 μm) as investigated in the literature [13,23]. A more detailed approach was also tested, using the van Rijn model that separates the bed-load from the suspended-load. In this case, the sediment forming the riverbed was represented with the two most frequent grain sizes, which were 125 and 250 μm. The bed-load contribution was attributed to the coarse fraction, whereas the suspended-load formula was applied to both of the grain sizes, enabling the graded model option.

In the preliminary tests, both of the sediment transport models were applied to grain sizes of 125–250 μm, with various discharges to cover the range observed in the period from 2004 to 2009, and the calibration coefficients (k in Eq. (6) and k_b and k_l in Eqs. (10) and (11)) were assumed equal to unity. The resulting sediment transport rates are reported in Fig. 7(a) for the total and the suspended-load formulae by Engelund–Hansen and van Rijn, respectively, and in Fig. 7(b) for the bed-load formula by van Rijn.

The same figures also reported evidence from the field campaigns corresponding to the Q_{ref} and regarding the suspended-load evaluation using the single and double-frequency approaches and the bed-load estimation using dune tracking.

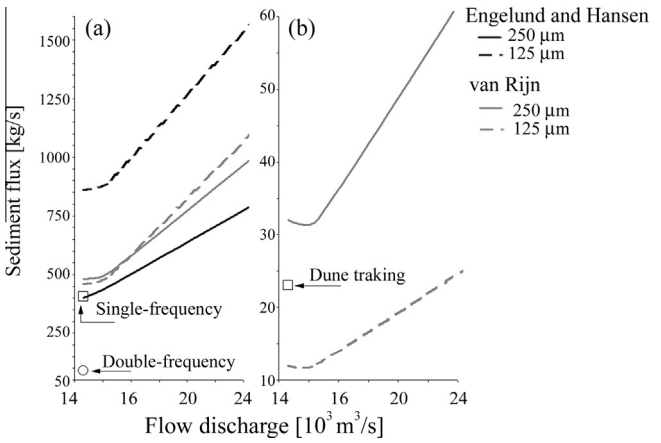

Fig. 7. The simulated sediment fluxes and corresponding data from the field; the total and suspended-load (a) were assessed with the Engelund–Hansen and van Rijn models, respectively, whereas the bed-load was estimated by using the van Rijn model (b).

Regarding the suspended-load, the single-frequency assessment agreed with the values from the Engelund–Hansen and van Rijn models, applied with 250 μm. This agreement explained the successful application of the Engelund and Hansen formula to estimate the total-load of the sediment spanning the entire sand range in the Parana River [13,23].

The van Rijn model was in relatively good agreement with the bed-load value from the dune tracking method.

The implementation of the Engelund and Hansen formula tended to overestimate the finer class load, which may depend on the simplified model applied to estimate the skin friction (Eq. (9)). In this case, the same Chézy parameter is applied in Eq. (9) to estimate the Shields parameter ϑ for the skin friction evaluation. The Chézy parameter was calibrated to account for the drag of the observed dunes; therefore, its combination with the Engelund and Hansen formula was inappropriate.

The long-term simulations, beginning in 2004, were performed with the un-coupled quasi-steady approach to evaluate the resulting bathymetry in 2009. This bathymetry was compared to the observed morphological changes in terms of the average erosions and depositions in the main and meandering channels (Figs. 8 and 9), and finally, the calibration coefficient in Eqs. (6), (10), and (11) were fixed. The reference dataset was derived from two bathymetric surveys performed in 2004 and 2009; the bed levels were interpolated and subtracted over the computational grid (Fig. 9(c)); finally, the average erosion and deposition were evaluated for the two channels.

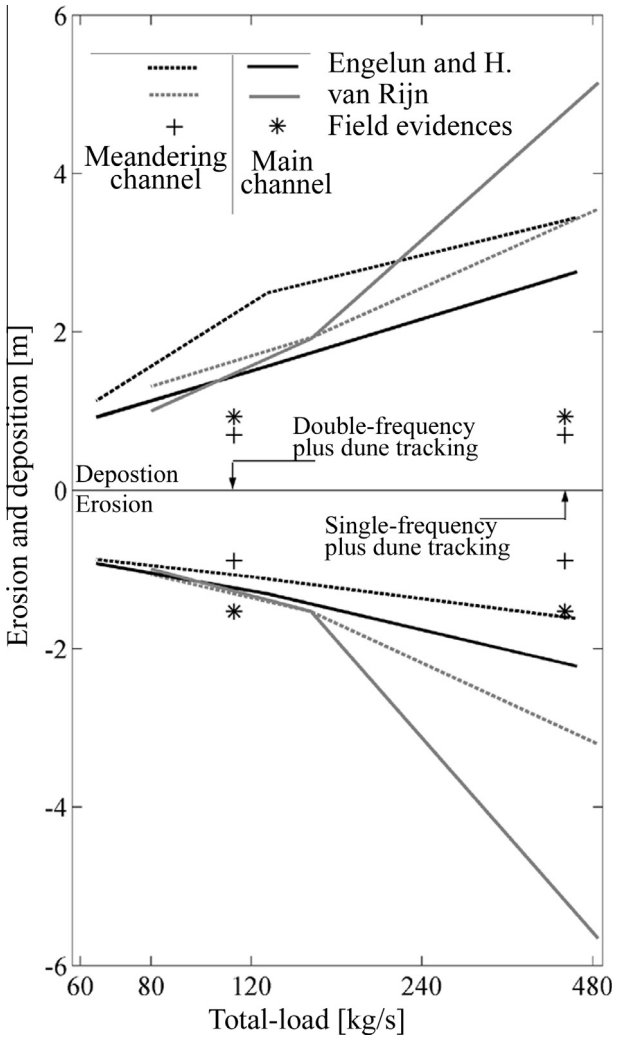

Fig. 8. Computed erosions and depositions in the main and meandering channels with various calibration coefficients in the sediment transport formulae (k in Eq. (6) and k_b and k_l in Eqs. (10) and (11)) and for flow discharge Q_{ref}: comparison with corresponding references from the field.

The relationship between the computed erosions and depositions and the simulated sediment transport rate related to the Q_{ref} and various values of k showed the influence of these calibration coefficients on the final morphology (Fig. 8).

The total-loads from the field campaign are reported in Fig. 8, with the y-axis corresponding to the reference erosions and depositions in the main and meandering channels. These total loads accounted for the dune tracking estimation for the bed-load and for the suspended-load assessment from the single- or double-frequency method.

The simulated erosions and depositions appeared overestimated, regardless of the applied transport formula, when considering the total-load of approximately 430 kg/s, which also corresponded to the suspended-load estimated by the single-frequency method. In contrast, the simulated averaged depositions and erosions were comparable to the observed values of approximately 1 m when the transport formulas were calibrated based on the estimated suspended-load of approximately 110 kg/s, as derived from the double-frequency method. The latter value was sensitive to the suspended sediments from the riverbed (i.e., with a grain size larger than 80–90 μm) that was represented in the numerical model. Given the objective of simulating the bed sediment morphodynamics, the sediment transport formulae were calibrated based on the double-frequency estimation to meet the observed erosions and depositions.

The best calibration was achieved with a k value of 0.15 in Eq. (6) for the single fraction (i.e., 250 μm) using the Engelund and Hansen formula. The van Rijn formulae were applied with the graded model. In this case, k_b in Eq. (10) was fixed to 1.4 and 0.0 for 250 μm and 125 μm, respectively, which accurately simulated the observed bed-load by applying the coarse fraction only. The calibration parameter k_l in Eq. (11) was set as 0.1 and 0.2 for 250 and 125 μm, respectively, accounting for the represented bed composition (i.e., 50–50% for 250–125 μm) and corresponding to a calibration parameter k_l of 0.15 as the average between the two classes.

Both of the applied sediment transport models provided relatively similar results when properly calibrated, but the depositions were more significantly overestimated in the meandering channel by the Engelund and Hansen formula (Fig. 8). This analysis fixed the best option to the van Rijn formulae coupled with the graded model.

3.4. Long-term morphology

The resulting bathymetry from the graded model and the van Rijn formulae better represented the progressive avulsion of the secondary channel observed passing from the 2004 to the 2009 morphology (Fig. 9). The river bars developing in the meandering channel were relatively well simulated, as follows: (i) the upstream bifurcation progressively recasting into a main-straight channel, (ii) the island protruding in the downstream portion of the meandering channel, which qualitatively agrees with the observed shoreline modifications (Fig. 3(b)).

The performed long-term simulations were less accurate in representing the development of the river bars in the main straight channel. In this case, the location of the bars close to the upstream and downstream junctions agreed with the observed morphological changes, but the simulated morphology showed larger depositions than those observed (Fig. 8). In addition, the bar between those junctions was simulated to develop on the left side of the main channel, whereas a developing alternate bars pattern was observed (Fig. 9(c)) passing from 2004 to 2009. However, the model captured the overall erosion tendency of the main channel.

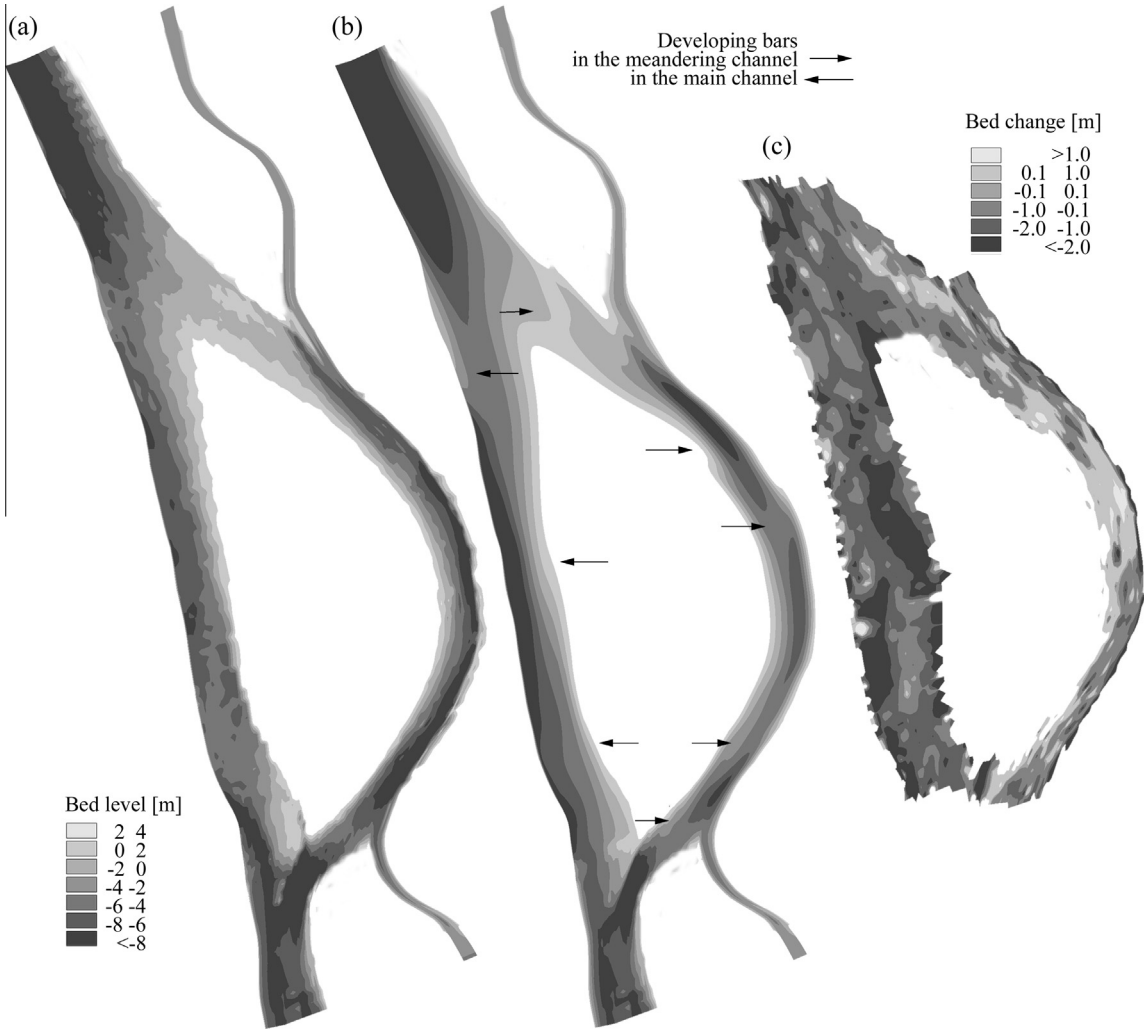

Fig. 9. The observed morphology in 2004 (a) as implemented in Mike21C, the 2009 morphology as resulting from the graded model simulation (b), and the observed erosion and deposition patterns from 2004 and 2009 bathymetries (c).

4. Discussion

The performed sensitivity analyses on the *md-m* un-coupling parameters and the sediment transport formulae enabled reliable simulations of the long-term morphodynamics of the Rosario reach with a quasi-steady approach. The morphological changes in this reach were preliminarily estimated with the river bar celerity on the order of 10^{-1} to 10^{-3} m per day, indicating that the morphological evolution was significantly slower than the hydrological yearly variations. Given this un-correlation between the morpho- and hydro-dynamic events, a 2-D model was applied with an un-coupled quasi-steady approach.

The shallow water approximation has been extensively applied in many numerical packages, such as in Mike21C. This simplification is particularly relevant to simulate large river morphodynamics at a scale of river bars and channel width, such as in the Parana River case study, in which the resolution of the computational grid was fixed based on the morphological scale rather than used to represent the hydrodynamic field variation along the water depth. This 100 m long morphological scale was 1–2 orders of magnitude larger than the turbulence scale in the vertical alignment, which is typically related to the water depth by applying the mixing length concept [48]. The average grid spacing of approximately 100 m properly represented the development of certain kilometres wide bars and channels and was fixed based on the observed dune wave length and the related macro-turbulence oscillations. In accordance with this approach, short scale processes, such as dune formation and propagation, were not directly represented, but their effects were accounted for with the calibrated horizontal eddy viscosity and the Chézy parameter.

Furthermore, the performed sensitivity analysis on the un-coupling parameters fixed the *md-ts* to 10^4 s, which is three orders of magnitude higher than the required *hd-ts* of 20 s to maintain a stable hydrodynamic computation with the Courant number close to four.

The ratio between the *md-ts* and the *hd-ts* gave an un-coupling rate of 10^3 for the performed simulations, which may be related to the water velocity over the bed-level celerity on the represented scale. This ratio reflected the morphological time scale length with respect to the time scale of the sediment transport into the flow (i.e., the morphodynamics to the sediment transport time scales ratio, the *md-st* ratio). In the analysed case study, the bed-level celerity was generally estimated on the order of 10^{-1} m/day as a maximum, which yielded 10^5 as the *md-st* ratio for the water velocity of approximately 1 m/s.

Moreover, the un-coupling rate was limited by the representation of the hydrological yearly variation. A quasi-steady approach was applied to simulate this variation with steady sub-periods of 20–25 days.

Table 2
Relationships between the model parameters and the observed flow and morphological features as order of magnitudes.

	Dunes wave length L (10^2 m)	Bars celerity C_b (10^{-1} m/day)	Bars wave length L_b (km)	Flow velocity u (m/s)	Flow vel. oscillation Δu (10^{-1} m/s)	Fl. vel. osc. period T (10^2 s)
Grid spacing 100 m	L		$10^{-1}\ L_b$			
Horizontal eddy scale 100 m	L			$T \cdot u$		$T \cdot u$
Horizontal eddy viscosity, *hev* 10 m^2/s	$L \cdot \Delta u$			$T \cdot u \cdot \Delta u$	$L \cdot \Delta u$	$T \cdot u \cdot \Delta u$
Morphodynamics to the sediment transport time scales ratio, *md-st* 10^5		u/C_b		u/C_b		

The low celerity of the morphological changes corresponded to the meagre rate of the sediment transport. However, the reliable modelling of the river morphodynamics over the period of 2004–2009 required an accurate estimation of the sediment fluxes; the long-term simulations accumulate relevant modifications of the riverbed. Thus, repeated surveys of the sediment transport rate should be applied to calibrate the morphodynamics models. Therefore, a first attempt was conducted in the Rosario reach in which the suspended-load was estimated from the echoes recording by the ADCPs, whereas dune tracking using the single-beam echo sonar provided a general estimation of the bed-load during the same campaign.

Particularly, referring to the suspended-load, the advantage of using the double-frequency method was to distinguish the grain size classes that better characterised the riverbed sediment (Fig. 2(c)), sorted from the entire range of the suspended sand. This process was particularly relevant to calibrate the transport formulae for the suspended-load in the applied morphodynamic model, which was aimed at representing the fluxes of the sediment forming the riverbed.

The higher sediment transport rate estimated with the single-frequency method compared with the double-frequency estimation may be ascribed to the overestimation of the evaluated backscatter. The backscatter from the fine fractions (i.e., 40–100 μm) was assumed to be equivalent to 100 μm backscatter, which appears to be oversimplified when considering the noticeable drop in the backscatter sensitivity for particles finer than 100 μm and using a 1200 kHz frequency [2]. Related to this limitation, the double-frequency method coupled the grain size classes with the corresponding concentrations in the backscatter evaluation and limited the measured range to the grain size fraction coarser than 80–90 μm.

In addition, the resulting migration velocity from the dune tracking method was applied to calibrate the van Rijn model for the bed-load. The application of this transport model also enabled separate evaluation for the bed and suspended-load, which gave a more accurate modelling.

The formula by Engelund and Hansen was successfully used by applying a single fraction corresponding to 250 μm to represent the sediment forming the riverbed (spanning the range of 100–300 μm), estimating relatively well the total-load of the fractions over the range of 40–300 μm. In addition to this inconsistency between the considered ranges of the grain size, the implementation of the Engelund and Hansen model in Mike21C entails a relevant oversimplification regarding the skin friction. The same Chézy parameter is used to estimate the dunes drag and the skin friction, which, for the case study, eventually yielded a significant overestimation of the finer fraction (125 μm) load and made the graded model option inappropriate.

5. Conclusions

The sand fluxes were investigated at a 2-km-wide bifurcation of the Lower Parana River near Rosario, Argentina, using acoustic technologies. Using the particles scattering at the two well-spaced frequencies of 600–1200 kHz ADCPs, the suspended-load was estimated discerning among the grain size classes from 80 to 300 μm. These grain sizes corresponded relatively well with the sediment fractions observed in the riverbed. Simultaneously, dune-tracking was applied using a single-beam echo-sounder to investigate the bed-load.

The estimations of the sediment fluxes from the field were applied to calibrate a 2-D numerical model. This calibration provided a reliable simulation of the observed erosions and depositions in the river channels. Furthermore, the bed-load estimation enabled the representation of the coarse fractions transported close to the bottom. In this case, the van Rijn model was applied to separate the bed from the suspended-load and provided consistent results with the observed morphological changes.

Although most of the transported sediment (i.e., clay, silt and very fine sand) was not observed in a significant amount in the riverbed, the entrainment of the coarse fractions in the full suspension from the bottom was a relevant mechanism to modify the riverbed morphology. Therefore, aiming to simulate these morphological changes, the 2-D numerical model was applied with an uncoupled quasi-steady approach that simulated the fluxes of these fractions. A sensitivity analysis was performed on the un-coupling parameters, which fixed the average mesh size and the morphodynamic module time step.

The grid longitudinal spacing of 100 m corresponded to the wave length of the observed oscillations in the horizontal plane. These oscillations referred to the dunes and the related macro-turbulence (i.e., the horizontal eddies scale), whereas the *md-ts* value of 3 h accounted for the estimated celerity of the river bars and the represented hydrological yearly variability. The relationships between these model parameters and the observed flow and morphological features are reported in Table 2 that may be considered for further applications regarding large rivers morphodynamics.

Given these results, further research efforts will be undertaken to accurately and widely investigate the fluxes of the sediment forming the riverbed for a better understanding of the river channel morphodynamics.

References

[1] Simmons SM, Parsons DR, Best JL, Orfeo O, Lane SN, Kostaschuk R, Hardy RJ, West G, Malzone C, Marcus J, Pocwiardowski P. Monitoring suspended sediment dynamics using MBES. J Hydraul Eng 2010;136(1):45–9. http://dx.doi.org/10.1061/ASCEHY.1943-7900.0000110.

[2] Guerrero M, Szupiany RN, Amsler ML. Comparison of acoustic backscattering techniques for suspended sediments investigations. Flow Measure Instrum 2011;22(5):392–401. http://dx.doi.org/10.1016/j.flowmeasinst.2011.06.003.

[3] Guerrero M, Ruther N, Szupiany RN. Laboratory validation of ADCP techniques for suspended sediments investigation. Flow Measure Instrum 2012;23(1):40–8. http://dx.doi.org/10.1016/j.flowmeasinst.2011.10.003.

[4] Guerrero M, Szupiany RN, Latosinski F. Multi-frequency acoustic for suspended sediment studies: an application in the Parana River. J Hydraul Res 2013;51(6):696–707. http://dx.doi.org/10.1080/00221686.2013.849296.

[5] Sassi MG, Hoitink AJF, Vermeulen B. Impact of sound attenuation by suspended sediment on ADCP backscatter calibrations. Water Resour Res 2012;48(9):W09520. http://dx.doi.org/10.1029/2012WR012008.

[6] Moore SA, Le Coz J, Hurther D, Paquier A. Using multi-frequency acoustic attenuation to monitor grain size and concentration of suspended sediment in rivers. J Acoust Soc Am 2013;133(4):1959–70. http://dx.doi.org/10.1121/1.4792645.

[7] Latosinski F, Szupiany RN, García CM, Guerrero M, Amsler ML. Estimation of concentration and load of suspended sediment in a large river by means of Doppler technology. J. Hydraul. Eng. 2014;140(7). http://dx.doi.org/10.1061/(ASCE)HY.1943-7900.0000859.
[8] Amsler ML, Ramonell CG, Toniolo HA. Morphologic changes in the Paraná River channel (Argentina) in the light of the climate variability during the 20th century. Geomorphology 2005;70(3):257–78. http://dx.doi.org/10.1016/j.geomorph.2005.02.008.
[9] Castro SL, Cafaro ED, Gallego MG, Ravelli AM, Alarcón JJ, Ramonell CG, Amsler ML. Evolución morfológica histórica del cauce del río Paranà en torno a Rosario (km 456–406). In: Proceedings of the CONAGUA 2007, Argentina [in Spanish]. http://hydriaweb.com.ar/kb/entry/122/, http://www.conicet.gov.ar/new_scp/detalle.php?keywords=&id=02622&inst=yes&congresos=yes&detalles=yes&congr_id=372052.
[10] Coleman JM, Roberts HH, Stone GW. Mississippi River delta: an overview. J Coastal Res, 0749-0208 1998;14(3):699–716. http://www.jstor.org/stable/4298830.
[11] Badano ND, Sabarots, Sabarots Gerbec M, Re M, Menéndez AN. A coupled hydro-sedimentologic model to assess the advance of the Parana River Delta Front. Proceedings of River Flow 2012, the International Conference on Fluvial Hydraulics, Costa Rica, 5–7 September 2012, 1. London, UK: Taylor & Francis Group; 2012, ISBN 9780415621298. p. 557–64. http://www.crcnetbase.com/doi/pdfplus/10.1201/b13250-86.
[12] Nones M, Ronco P, Di Silvio G. Modelling the impact of large impoundments on Lower Zambezi River. Int J River Basin Manage 2013;11(2):221–36. http://dx.doi.org/10.1080/15715124.2013.794144.
[13] Nones M, Guerrero M, Ronco P. Opportunities from low-resolution modelling of river morphology in remote parts of the world. Earth Surf Dyn 2014;2(1):9–19. http://dx.doi.org/10.5194/esurf-2-9-2014.
[14] Schweitzer AM. La ciudad de Victoria en proceso de transformación: turismo y nuevos emprendimientos a partir de la construcción del enlace Rosario-Victoria. In: Turismo, pobreza y territorios en América Latina: Bogotá. Colombia: Universidad Externado de Colombia; 2008, ISBN 978-958-710-361-8. p. 151–76. http://EconPapers.repec.org/RePEc:ext:hotele:14.
[15] Guerrero M, Re M, Kazimierski LDD, Menéndez AN, Ugarelli R. Effect of climate change on navigation channel dredging of the Parana River. Int J River Basin Manage 2013;11(4):439–48. http://dx.doi.org/10.1080/15715124.2013.819005.
[16] Szupiany RN, Amsler ML, Best JL, Parsons DR. Comparison of fixed and moving vessel flow measurements with an aDp in a large river. J Hydraul Eng 2007;133(12):1299–309. http://dx.doi.org/10.1061/(ASCE)0733-9429(2007)133:12(1299.
[17] Guerrero M, Di Federico V, Lamberti A. Calibration of a 2-D morphodynamic model using water-sediment flux maps derived from an ADCP recording. J Hydroinf 2013;15(3):813–28. http://dx.doi.org/10.2166/hydro.2012.126.
[18] Guerrero M. The investigation of sediment processes in rivers by means of the Acoustic Doppler Profiler. In: Proceedings of Evolving Water Resources Systems: Understanding, Predicting and Managing Water–Society Interactions, Bologna, Italy: IAHS; 2014. p. 364: 368–373. ISBN 978-1-907161-42-1, http://iahs.info/uploads/dms/16529.Guerrero-Abs-61.pdf.
[19] Haun S, Rüther N, Baranya S, Guerrero M. Comparison of real time suspended sediment transport measurements in river environment by LISST instruments in stationary and moving operation mode. Flow Measure Instrum 2015;41:10–7. http://dx.doi.org/10.1016/j.flowmeasinst.2014.10.009.
[20] Guerrero M, Rüther N, Archetti R. Comparison under controlled conditions between multi-frequency ADCPs and LISST-SL for investigating suspended sand in rivers. Flow Measure Instrum 2014;37:73–82. http://dx.doi.org/10.1016/j.flowmeasinst.2014.03.007.
[21] Parsons DR, Best JL, Orfeo O, Hardy RJ, Kostaschuk R, Lane SN. Morphology and flow fields of three dimensional dunes Rio Paranà Argentina: results from simultaneous multibeam echo sounding and acoustic Doppler current profiling. J Geophys Res 2005;110:F04S03. http://dx.doi.org/10.1029/2004JF000231.
[22] Guerrero M, Lamberti A. Flow field and morphology mapping using ADCP and multibeam techniques: survey in the Po River. J Hydraul Eng 2011;137(12):1576–87. http://dx.doi.org/10.1061/(ASCE)HY.1943-7900.0000464.
[23] Guerrero M, Lamberti A. Bed-roughness investigation for a 2-D model calibration: the San Martìn case study at Lower Paranà. Int. J Sediment Res 2013;28(4):458–69. http://dx.doi.org/10.1016/S1001-6279(14)60005-6.
[24] Szupiany RN, Amsler ML, Parsons DR, Best JL. Morphology, flow structure, and suspended bed sediment transport at two large braid-bar confluences. Water Resour Res 2009;45:W05415. http://dx.doi.org/10.1029/2008WR007428.
[25] Simons DB, Richardson EV, Nordin CF. Bedload equation for ripples and dunes. US Geol Surv Prof Pap 1965;462-H:1–9. http://pubs.er.usgs.gov/publication/pp462H, http://pubs.usgs.gov/pp/0462h/report.pdf.
[26] Engel P, Lau YL. Computation of bedload using bathymetric data. Proc Am Soc Civ Eng, 0044-796X 1980;106(3):369–80.
[27] Harbor DJ. Dynamics of bedforms in the lower Mississippi River. J Sediment Res 1998;68(5):750–62. http://archives.datapages.com/data/sepm/journals/v66-67/data/068/068005/0750.HTM.
[28] Wilbers AWE, Ten Brinke WBM. The response of subaqueous dunes to floods in sand and gravel bed reaches of the Dutch Rhine. Sedimentology 2003;50(6):1013–34. http://dx.doi.org/10.1046/j.1365-3091.2003.00585.x.
[29] Duffy GP, Hughes-Clarke JE. Application of spatial cross correlation to detection of migration of submarine sand dunes. J Geophys Res F: Earth Surf 2005;110(4):F04S12. http://dx.doi.org/10.1029/2004JF000192.
[30] Nittrouer JA, Allison MA, Campanella R. Bedform transport rates for the lowermost Mississippi River. J Geophys Res F: Earth Surf 2008;113(3):F03004. http://dx.doi.org/10.1029/2007JF000795.
[31] DHI Water & Environment. Mike21C river hydrodynamics and morphology user guide. DHI, Horsholm, Denmark; 2002. http://www.dhigroup.com/upload/dhisoftwarearchive/shortdescriptions/wr/m21c_short_2004.pdf.
[32] Engelund F, Hansen E. A monograph on sediment transport in alluvial streams. Copenhagen, Denmark: Teknisk Vorlag; 1967. http://repository.tudelft.nl/assets/uuid:81101b08-04b5-4082-9121-861949c336c9/Engelund_Hansen1967.pdf.
[33] van Rijn LC. Part I: Bed load transport. J Hydraul Eng 1984;110(10):1431–56. http://dx.doi.org/10.1061/(ASCE)0733-9429(1984) 110:10(1431.
[34] van Rijn LC. Part II: Suspended load transport. J Hydraul Eng 1984;110(11):1613–41. http://dx.doi.org/10.1061/(ASCE)0733-9429(1984)110:11(1613.
[35] Latrubesse EM. Patterns of anabranching channels: the ultimate end-member adjustment of mega rivers. Geomorphology 2008;101:130–45. http://dx.doi.org/10.1016/j.geomorph.2008.05.035.
[36] Orfeo O, Stevaux J. Hydraulic and morphological characteristics of middle and upper reaches of the Paranà River (Argentina and Brazil). Geomorphology 2002;44(3):309–22. http://dx.doi.org/10.1016/S0169-555X(01)00180-5.
[37] Ramonell CG, Amsler ML, Toniolo H. Shifting modes of the Parana River thalweg in its middle/lower reach. In: South and Central American Rivers, Zeitschr. Geomorphol. 2002, ISBN 978-3-443-21129-5. p.129–42. https://www.schweizerbart.de/publications/detail/isbn/9783443211295/Zeitschr_f_Geomorphologie_Suppl_Bd_1#t8310.
[38] Gaeuman G, Jacobson RB. Field assessment of alternative bed-load transport estimators. J Hydraul Eng 2007;133(12):1319–28. http://dx.doi.org/10.1061/(ASCE)0733-9429(2007)133:12(1319).
[39] Olesen KW. Bed topography in shallow river bends. Commun Hydraul 1987;87(1):1–265. Dept. of Civil Engineering, Delft Univ. of Technology, The Netherlands, http://repository.tudelft.nl/assets/uuid:e9b7082e-76dc-407d-a334-3d9e471d5a93/TR%20DISS%201566%281%29.PDF.
[40] Talmon AM. Bed topography of river bends with suspended sediment transport [Ph.D. thesis]. Delft Univ. of Technology, The Netherlands; 1992. http://repository.tudelft.nl/view/ir/uuid:bd4cdc3e-a4f5-4ba9-977a-1fb9a420f0d0/.
[41] Shields A. Application of similarity principles and turbulence research to bed-load movement. In: Ott WP, Uchelen JC, translators. Mitt. Preuss. Verschsanst., Berlin. Wasserbau Schiffbau 1936, California Institute of Technology, Pasadena, CA, Report No. 167, p. 43. http://resolver.caltech.edu/CaltechKHR:HydroLabpub167.
[42] Rouse H. Fluid mechanics for hydraulic engineers. New York: Dover Publications; 1961. republished by Read Books 2011, ISBN 1447438809, 9781447438809.
[43] USGS database, EarthExplorer; 2014. http://earthexplorer.usgs.gov/.
[44] Guerrero M, Nones M, Saurral R, Montroull N, Szupiany RN. Parana River morphodynamics in the context of climate change. Int J River Basin Manage 2013;11(4):423–37. http://dx.doi.org/10.1080/15715124.2013.826234.
[45] Aricó C, Sinagra M, Begnudelli L, Tucciarelli T. MAST-2D diffusive model for flood prediction on domains with triangular Delaunay unstructured meshes. Adv Water Res 2011;34:1427–49. http://dx.doi.org/10.1016/j.advwatres.2011.08.002.
[46] Yalin MS, Da Silva AM. Fluvial processes. IAHR Monographs. London: Taylor & Francis; 2015. ISBN 1138001384, 9781138001381.
[47] Tennekes H, Lumley JL. A first course in turbulence. Cambridge: MIT Press; 1972, ISBN 9780262200196.